The Journal of Chemical Physics

New aspects of operando Raman spectroscopy applied to electrochemical CO_2 reduction on Cu foams

Cite as: J. Chem. Phys. **150**, 041718 (2019); https://doi.org/10.1063/1.5054109
Submitted: 29 August 2018 . Accepted: 31 October 2018 . Published Online: 20 December 2018

Shan Jiang, Katharina Klingan, Chiara Pasquini, and Holger Dau

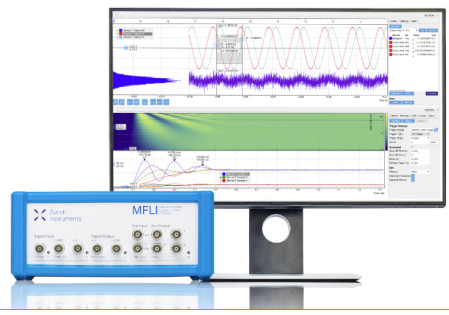

The Journal of Chemical Physics ARTICLE scitation.org/journal/jcp

New aspects of operando Raman spectroscopy applied to electrochemical CO_2 reduction on Cu foams

Cite as: J. Chem. Phys. 150, 041718 (2019); doi: 10.1063/1.5054109
Submitted: 29 August 2018 • Accepted: 31 October 2018 •
Published Online: 20 December 2018

Shan Jiang,[a] Katharina Klingan,[a),b)] Chiara Pasquini, and Holger Dau[b)]

AFFILIATIONS

Department of Physics, Freie Universität Berlin, Arnimallee 14, 14195 Berlin, Germany

[a)]S. Jiang and K. Klingan contributed equally to this work.
[b)]Authors to whom correspondence should be addressed: katharina.klingan@fu-berlin.de and holger.dau@fu-berlin.de

ABSTRACT

The mechanism of electrochemical CO_2 reduction (CO_2RR) on copper surfaces is still insufficiently understood. *Operando* Raman spectroscopy is ideally suited to elucidate the role of adsorbed reaction intermediates and products. For a Cu foam material which has been previously characterized regarding electrochemical properties and product spectrum, 129 *operando* spectra are reported, covering the spectral range from 250 to 3300 cm^{-1}. (1) The dendritic foam structure facilitates surface-enhanced Raman spectroscopy (SERS) and thus electrochemical *operando* spectroscopy, without any further surface manipulations. (2) Both Raman enhancement and SERS background depend strongly on the electric potential and the "history" of preceding potential sequences. (3) To restore the plausible intensity dependencies of Raman bands, normalization to the SERS background intensity is proposed. (4) Two distinct types of *CO adsorption modes are resolved. (5) Hysteresis in the potential-dependent *CO desorption supports previous electrochemical analyses; saturating *CO adsorption may limit CO formation rates. (6) HCO_3^- likely deprotonates upon adsorption so that exclusively adsorbed carbonate is detectable, but with strong dependence on the preceding potential sequences. (7) A variety of species and adsorption modes of reaction products containing C—H bonds were detected and compared to reference solutions of likely reaction products, but further investigations are required for assignment to specific molecular species. (8) The Raman bands of adsorbed reaction products depend weakly or strongly on the preceding potential sequences. In future investigations, suitably designed potential protocols could provide valuable insights into the potential-dependent kinetics of product formation, adsorption, and desorption.

I. INTRODUCTION

The massive use of fossil fuels to cover the globally rising energy demand has resulted in dramatically increasing atmospheric CO_2 levels, thereby promoting global climate change. An attractive strategy to mitigate CO_2 emissions is electrochemical CO_2 reduction (CO_2RR) for the production of energy-rich compounds or commodity chemicals in general.[1–5] If coupled to renewable energy sources, specifically wind or solar energy, fossil fuels can be replaced without increasing the atmospheric CO_2 load further. Efficient and product-specific electrochemical CO_2RR requires rationally optimized catalyst materials. However, mechanistically, CO_2RR is clearly insufficiently understood, in spite of major scientific advancements.[6–21] Elucidation of the crucial reaction mechanism can be supported by the implementation of experimental *operando* techniques, which can detect educts, products, and possibly reaction intermediates during electrochemical operation of the catalyst material.

Vibrational spectroscopy, specifically surface-enhanced Raman spectroscopy (SERS), can be readily coupled to an electrochemistry experiment and thereby becomes a promising experimental tool in CO_2RR research, given the sensitivity to identify adsorbate species and their

bonding to the surface.[22–27] *Operando* SERS has the potential to probe molecules adsorbed on the surface with high sensitivity during the operation of the catalysts at various electrical potentials and electrolyte compositions. Copper electrodes are of high interest for CO_2RR,[4,28–32] and rough Cu surfaces are well-known for the surface enhancement of Raman intensities.[2,33–36] The intensity amplification is due to the electric field enhancement occurring in the vicinity of resonantly irradiated Cu particles with localized surface plasmons.[37]

Operando Raman spectroscopy has not been used very frequently for the detection of surface-adsorbed molecules in aqueous CO_2 reduction, possibly related to specific challenges involved in *operando* SERS. The technique requires suitably structured "rough" surfaces, SERS background signals may distort the spectral information,[38–40] intense gas evolution at higher overpotentials can impede the measurements, and a variety of Raman peaks may complicate the interpretation of the Raman spectra seriously. Nonetheless, *operando* SERS is well-suited to follow the chemical state of surface metal ions and to identify molecular species adsorbed at the catalytic electrode.[29,42–45] Focusing on the metal and metal oxide bands in a smaller wavenumber range simplifies data interpretation but also restricts the potential insights. Attempts to fully describe potential-dependent reaction intermediates employing an extended wavenumber range during aqueous CO_2RR via *operando* Raman spectroscopy are rare.[46,47] The analysis of adsorbed CO (*CO), a prominent CO_2RR intermediate, is a promising exception.[44,48–51] Reversible *CO-induced surface reconstruction of a Cu surface has been observed under catalytic conditions.[48] On mixed Cu—Au surfaces, variations in relative peak intensities have been linked to relative *CO surface concentrations and shifts of the C≡O stretching mode (peak around 2100 cm^{-1}) to lower wavenumbers have been linked to longer C—O bonds (effect of the local electrostatic field–electrochemical Stark effect[52,53]) and to stronger metal-CO interactions.[49] In future, it could be possible to derive bonding strengths and lengths of metal-chemisorbed *CO clusters during CO_2RR via the combination of density functional theory (DFT) and *operando* Raman spectroscopy, similar to Ref. 54.

In this work, we address the complicated background phenomena and undertake first steps in the investigation of the adsorbed reaction species at the surface of a Cu foam electrode during electrochemical CO_2 reduction. Additionally, we identify the chemical state of the Cu electrode surface, specifically the potential-dependence of oxide formation. A highly porous electrodeposited Cu foam was employed, because of its interesting CO_2RR properties, which has previously been well-characterized regarding structural parameters and the CO_2RR product spectrum.[32] High surface area Cu foams have a product distribution that differs distinctly from the product distribution of a flat Cu metal surface: formation of hydrogen and methane is strongly suppressed (per surface area), whereas carbon monoxide and even more so ethylene are formed with especially high partial current densities.[32] Limitation of the proton transport and alkalization at the foam surface, as verified by Raman spectroscopy on the bicarbonate buffer solution, may explain this selectivity shift, as discussed elsewhere.[32] In the present work, we show that the interesting Cu-foam catalysts excel by another property: they provide a SERS-active surface in their "native" as-synthesized form.

II. RESULTS AND DISCUSSION

The experiments were performed in a confocal Raman spectrometer equipped with a home-built 3-electrode electrochemical cell using a water-immersion objective and excitation at 633 nm, as detailed in the supplementary material. By employing a laser power of 1.3 mW in combination with a line focus (~100 μm length), the laser intensity was kept at a low level; no indication for any irradiation-induced modifications was detected. Throughout the individual experiments, the electrolyte (0.1M $KHCO_3$, pH 6.8) was constantly purged with gaseous CO_2. Cu foams were freshly electrodeposited from 0.2M $CuSO_4$/1.5M H_2SO_4 solution for 20 s at −0.5 A cm^{-2} as described in Ref. 32, cleaned, and used for Raman experiments within the same day.

The aims of this work are (i) to scrutinize the potential-dependent Raman background phenomenon described in Refs. 40, 55, and 56, (ii) to identify the chemical surface state of the Cu foam electrode during CO_2RR (oxide versus metallic surface), and (iii) to follow the adsorption of different molecular intermediate and product species during CO_2RR. Therefore, we performed the following experimental series:

(1) *Series* 1. Using a freshly electrodeposited Cu foam, we decreased the applied potentials from 0 to −0.9 V_{RHE} in 100 mV steps (20 s of equilibration and 30 s of data collection at each potential), for tracking the electrochemical reduction of the Cu-foam surface to metallic Cu. Directly after this experiment, we exchanged the bicarbonate electrolyte against fresh buffer solution.
(2) *Series* 2. After Series 1, we applied potentials from −0.1 to −0.9 V_{RHE} in 100 mV steps to investigate the accumulation of adsorbate species before the onset of CO_2RR (>−0.6 V_{RHE}) and reaction intermediates/products during CO_2RR (≤−0.6 V_{RHE}).
(3) *Series* 3. Directly after Series 2 of increasingly negative potentials, we stepped the potential upwards (−0.8 to −0.1 V_{RHE} in 100 mV steps) to follow the desorption behavior.

The raw data of this experimental series are shown in Fig. 1. Complex potential-dependent changes in the intensity of a broad background and several sharp Raman bands were observed. The potential-dependence is intricate, but as a general trend, the low-potential background is smaller than the high-potential background. This trend is

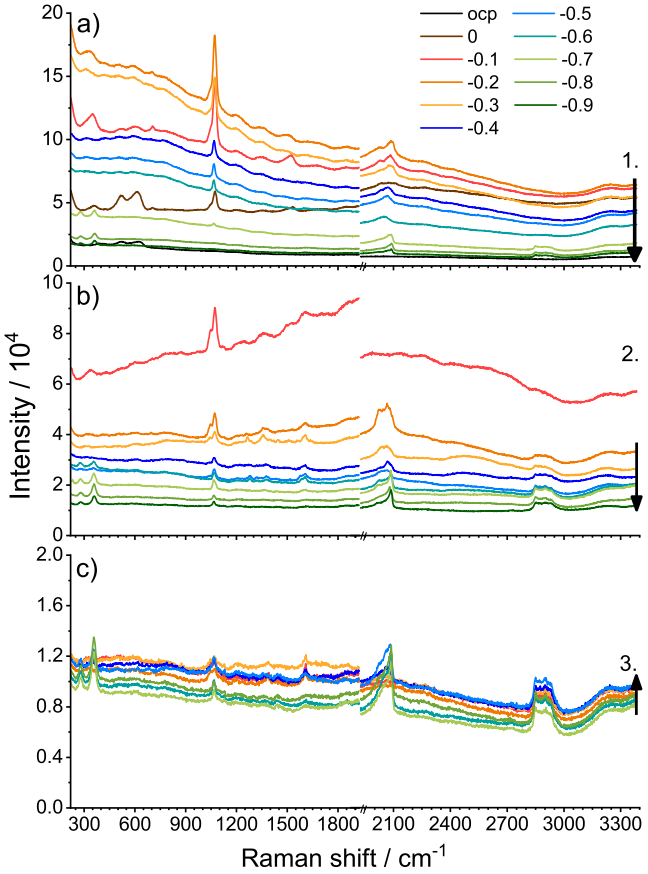

FIG. 1. *Operando* Raman spectra of Cu foam in CO_2-saturated $KHCO_3$ buffer (0.1M, pH 6.8) at various electrochemical potentials, before background subtraction and normalization. (a) Reduction of Cu_xOH_y to metallic copper and electrochemical CO_2 reduction from 0 to −0.9 V_{RHE} (Series 1, as described in the main text). (b) After oxide reduction, potentials from −0.1 to −0.9 V_{RHE} were applied (Series 2). (c) Backward scan from −0.8 to −0.1 V_{RHE} (Series 3). Arrows indicate the scan direction of the electric potential. The legend in panel (a) provides the applied potentials (vs. RHE) and the respective line color; the black line labeled by "*ocp*" corresponds to conditions of an "open-circuit potential" meaning that no potential was applied at the "floating" working electrode. The spectra are NOT offset. The zero-level of the Raman intensity was estimated from a H_2O solution spectrum and found to be negligibly small (below 5×10^2 counts, Fig. S1).

in line with previous findings that the SERS background intensity depends on the electrochemical potential.[40,55,56] The strong background in the raw data spectra impedes a straightforward interpretation of specific SERS bands and intensities and requires for appropriate offset subtraction and normalization. In any event, the clearly distinguishable Raman bands reveal that this type of Cu foam[57–60] with high electrochemical surface areas (>30 cm^2 per 1 cm^2 of the planar electrode surface) is an excellent SERS-active substrate that does not require any further surface modification.

Figure 2 shows the potential-dependent intensities of the SERS background. During experimental Series 1 and 2,

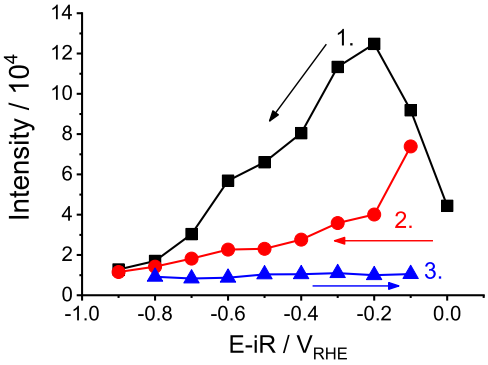

FIG. 2. Intensity of the SERS background (averaged values of region 1) versus electrochemical potential of a Cu foam in 0.1M $KHCO_3$ (pH 6.8). The black symbols correspond to Series 1 (increasingly negative potentials), the red symbols correspond to Series 2 (second series of increasing negative potentials), and the blue symbols correspond to Series 3 (increasingly positive potentials). The background intensities relate to the data shown in Fig. 1.

the background intensities decrease strongly with increasingly negative potential, whereas in Series 3 this trend is clearly weaker. These results indicate that the potential-dependence of the background is also determined by the history of exposures to various potentials, as also found in Ref. 40. The history of applied electric potentials may have affected the background by causing disappearance of oxide domains, not rapidly reversible coverage with adsorbed molecules, and irreversible modifications of the surface nanostructure.

To separate the broad background from the SERS peaks, we subtracted polynomial functions and then normalized the Raman intensities to the background intensity, as detailed in the supplementary material. Normalization was done by averaging the intensity of the background curve, and the averaged (integrated) background intensity was used to divide the spectra. The obtained spectra are shown in Fig. 3 (subtracted background spectra in Fig. S2 and normalization factors in Table S1). However, the peak intensities without background normalization exhibit a more or less chaotic potential-dependence (Fig. 1), whereas the background normalization results in a reasonably regular potential-dependence of the peak intensities (Fig. 3). Therefore, we suggest that not only background subtraction but also suitable normalization of the potential-dependent SERS Raman data is an essential step before the interpretation of trends in the peak intensities can be approached.

We note that an alternative option for background subtraction and normalization has been proposed and verified in an elegant study of Ren and co-workers,[41] which involves the correlation of the photoluminescence (PL) with the SERS background. In the current study, we obtained plausible results with the normalization protocol described above, which may be more approximate, but excels by simplicity.

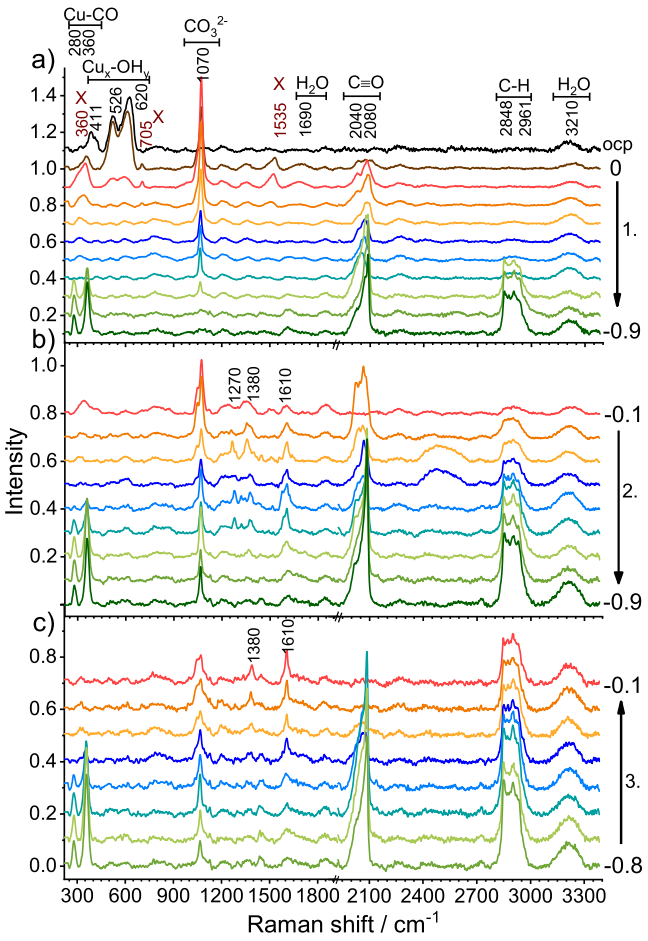

FIG. 3. *Operando* Raman spectra of Cu foam in CO_2-saturated $KHCO_3$ buffer (0.1M, pH 6.8) at various electrochemical potentials, after background subtraction and normalization. The data of Fig. 1 were processed by background subtraction and normalization to the intensity of the SERS background; for clarity of the graphical presentation, a vertical offset was applied. (a) Reduction of Cu_xOH_y to metallic copper and electrochemical CO_2 reduction by potentials ranging from 0 to −0.9 V_{RHE} (Series 1). (b) After oxide reduction, potentials from −0.1 to −0.9 V_{RHE} were applied (Series 2). (c) Backward scan from −0.8 to −0.1 V_{RHE} (Series 3). The water band at 3210 cm^{-1} corresponds to the broad spectrum of O—H stretching vibrations (3000-3700 cm^{-1}, Fig. S1) which becomes visible as a separate band only after the removal of a smooth background; it likely results from bulk water molecules and thus is not informative in the context of the present study.

After background subtraction and normalization, we observe—aside from comparably sharp SERS bands assignable to surface oxides or molecular species—broad, often regularly spaced peaks in all spectra (Fig. 3). A Raman spectrum of a paper sheet shows a wide fluorescence signal with largely the same oscillatory background; a spectrum of air does not show such features (Fig. S3). Subtraction of the scaled paper spectrum from the spectra of Fig. 3 reduces the oscillatory background significantly [Fig. S4(b)]. These experiments clarify that the approximately oscillatory background is unrelated to the SERS signals and represents merely an (irrelevant) artefact of the detection system. In our present study, we do not subtract the oscillatory background because the comparably sharp SERS bands are not seriously affected.

For repetitions of Cu-foam electrodeposition and Raman measurement on the freshly electrodeposited Cu foams, we observed (minor) fluctuations in the background-subtracted and normalized intensities of the Raman bands, as exemplarily shown in Fig. S5. The intensity deviations after background normalization could come from the variability of the optical and morphological properties of the irradiated Cu foam surface resulting, e.g., in differences in the orientation of adsorbed molecules relative to the polarized Raman laser beam. We note that, taking into account the complex morphology with dendritic structures and irregular pores, the reproducibility is surprisingly good. Aside from the used normalization, the selection of comparably planar surface spots and spatial averaging achieved by using a line focus of about 100 μm length are factors that certainly contribute to good reproducibility.

Before discussing the reactions and processes related to CO_2 reduction reaction, we address the formation and disappearance of Cu oxides in more detail. Therefore, Raman spectra were collected during slow cyclic voltammetry (CV) (1 mV s^{-1}) covering the potential range from −0.4 V_{RHE} to +0.9 V_{RHE} (Fig. 4).

A. Copper oxides

Minimally four distinct SERS bands below 750 cm^{-1} are visible in the Series 1 spectra of Fig. 3 recorded without the applied electric potential (*ocp*) or at high potentials, which are likely assignable to Cu oxides or hydroxides. To shine more light on the identity of the observed Cu_x—OH_y bands, we scanned the Cu foam in 0.1M $KHCO_3$ pH 8.8 with 1 mV s^{-1} from negative to positive potentials, in a potential range where the transformation of metallic Cu^0 to Cu^I oxide and Cu^{II} oxide species is anticipated (Raman spectra in Fig. 4, CV in Fig. S6). From the original, background-dominated spectra [Figs. 4(a) and 4(b)], informative Raman bands were extracted by background subtraction and normalization [Figs. 4(c) and 4(d)], using the same protocol described for the spectra of Fig. 3. The bands at 411, 520, and 600-622 cm^{-1} are visible in the forward and backward scan. The spectra of the backward scan exhibit new bands at 360 and 705 cm^{-1}, indicating the formation of another species not detectable during the forward scan.

When advancing from negative to highly positive potentials [from −0.4 to 0.90 V_{RHE} in Fig. 4(a)], the background decreases pronouncedly, by a factor of about six. During the backward scan [Fig. 4(b)], when decreasing the potential, the background intensity increases drastically to a level that is about four times greater than the starting level of the forward scan (around 0 V_{RHE}) before decreasing to a level that is close to the starting level (at −0.35 V_{RHE}). The chemical species associated with the bands at 360 and 705 cm^{-1} may be related to the especially strong background signal observed during the backward scan around 0 V_{RHE}.

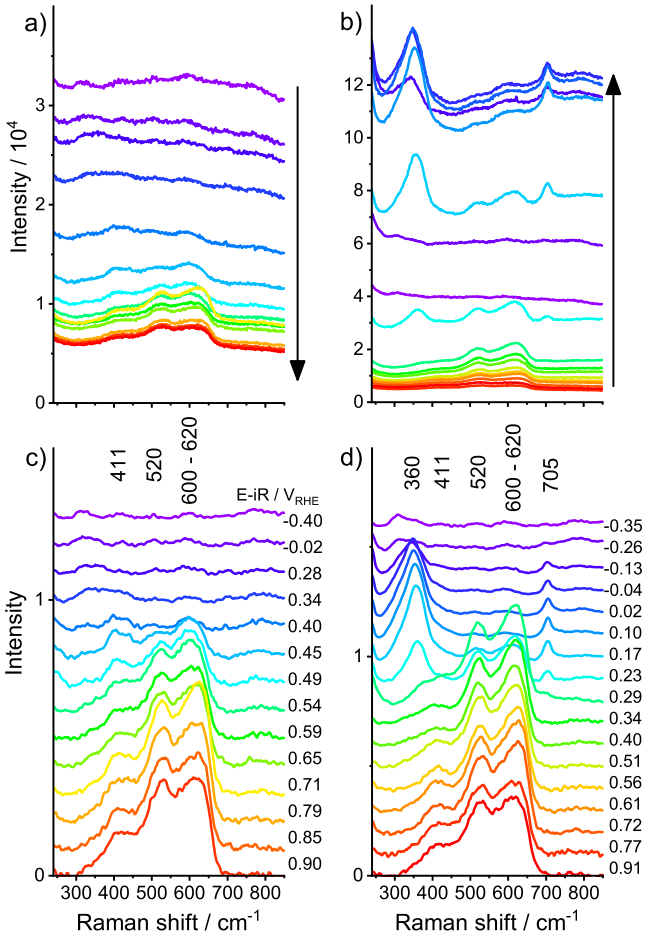

FIG. 4. *Operando* Raman spectra at various electrochemical potentials of a Cu foam during a CV with 1 mV s^{-1} (0.1M $KHCO_3$ buffer, pH 8.8). In (a) and (c), forward-scan from negative to positive potentials. In (b) and (d), backward-scan from positive to negative potentials. The top row of spectra, in (a) and (b), shows the unprocessed data; the spectra are NOT offset. The arrows indicate the direction of major changes in the Raman intensity during the scan of the electric potential. The bottom row of spectra, in (c) and (d), shows the background-subtracted and normalized spectra; a vertical offset was applied for visual clarity.

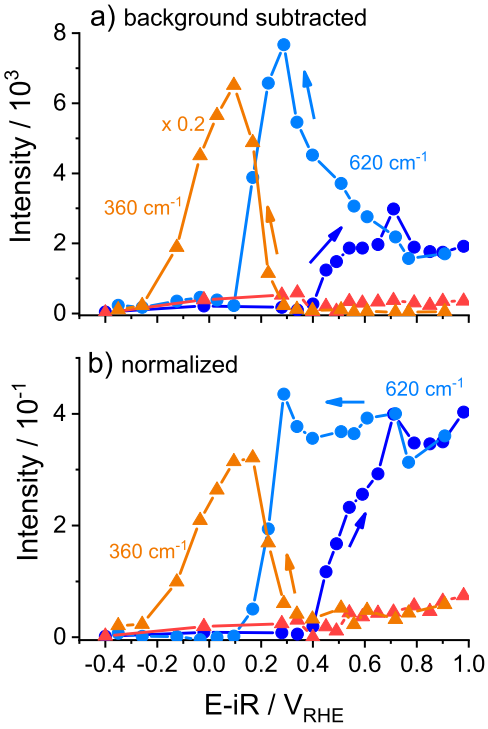

FIG. 5. Potential dependent Raman intensities at 620 cm^{-1} (dark and light blue) and at 360 cm^{-1} (red and orange) of a Cu foam during a CV with 1 mV s^{-1} in 0.1M $KHCO_3$ (pH 8.8). (a) Background subtracted intensities. (b) Background subtracted and normalized intensities. Arrows indicate the potential scan direction. The intensities relate to the data shown in Fig. 4. The backward-scan intensities (orange curve) in (a) have been multiplied by 0.2.

Comparison of Figs. 4(b) and 4(d) reveals the need for background normalization. In Fig. 4(b), the band intensities between 350 and 700 cm^{-1} increase strongly for lowering of the electric potential, which is opposite to the expected behavior. After normalization [Fig. 4(d)], these bands stay approximately constant until the potential drops below 0.29 V, which represents the expected behavior, as clearly visible in Fig. 5. We conclude that background subtraction without normalization can result in misleading trends in the potential-dependence of the intensity of the SERS band, whereas normalization by the SERS background leads to a plausible behavior.

Cu_2O is known to have bands around 415,[61] 525,[43,62–64] and 625 cm^{-1}.[29,62–65] Similar peaks are observed for the Cu foam from 0.45 to 0.90 V_{RHE} during the forward scan, and from 0.91 to 0.29 V_{RHE} during the backward scan (Figs. 4 and 5). In clear contrast, CuO is known to have a high intensity peak at 288 cm^{-1} and one with lower intensity at 337 cm^{-1},[29,62,63,66,67] but we never observe these Raman bands. $Cu(OH)_2$ Raman bands at about 292 and 483 cm^{-1} have been reported,[62] but also these bands were not detectable. However, oxidation of the Cu foam beyond Cu^I species may result in a layer consisting of mixed oxidation states and phases, likely as a Cu_2O—CuO—$Cu(OH)_2$ layer.[68,69] A potential-dependence of structure and composition of these oxides layers could explain the blue shift from 600 cm^{-1}, at lower potentials, to 622 cm^{-1} at higher potentials.

In a recent study on roughened Cu surfaces, the species observed at 360, 705, and 1535 cm^{-1} (see Fig. S7 for Raman data on an extended scale) were assigned to adsorbed carboxylate CO_2^-, a possible intermediate in the formate production path.[70] The authors concluded from ^{13}C isotopic shift experiments and DFT calculations that the band at 1535 cm^{-1} represents an out of surface C—O stretching mode, while the bands at 360 and 705 cm^{-1} are mostly present as stretching mode of the Cu—C bond and in-plane bending of CO_2^-, respectively.[70] Similar to Ref. 70, we observed the presence

of these three bands only after all oxide species had been reduced by the application of a series of increasingly negative electrode potentials (Figs. 4 and 5). Starting from reduced Cu foams, these peaks are not detectable. Therefore, we tentatively assume that the formation of the bands at 360, 705, and 1535 cm^{-1} (labeled "X" in Fig. 3) is closely linked to the reduction of oxide species, originating possibly from interactions of carbonate or CO_2 with the defect sites of the Cu material transiently formed at intermediate electrode potentials.

Regarding use of Cu foams for the reduction of CO_2 (Fig. 3), we conclude that the reduction of Cu_2O and possibly mixed oxy-hydroxide phases is completed at −0.1 V_{RHE} and the reduction of further carboxylate related intermediates likely is completed at −0.4 V_{RHE}. There are no indications of any surface oxides at potentials that are typically employed for CO_2 reduction.

B. Carbon monoxide adsorption

We observe four different Raman bands related to CO, at about 280, 360, 2040, and 2080 cm^{-1} (Fig. 6). The two low-frequency bands are characteristic for Cu—CO vibrations: at 280 cm^{-1} the frustrated rotational mode of CO, and at 360 cm^{-1} the Cu—CO stretch vibration (atop geometry).[48,72,73] The two high-frequency bands are assignable to intramolecular C≡O stretching vibrations with different adsorption geometries.[48,72,73] We generally detect CO vibrations only after reduction of the Cu surface oxides, suggesting that electrochemical CO_2 reduction is not promoted by oxide species but takes place at metallic Cu sites.

Intramolecular C≡O stretch bands are already present at a potential as high as −0.2 V_{RHE}. Between −0.1 and −0.4 V_{RHE}, an asymmetric broad band around 2040 cm^{-1} (ranging from about 1980 to 2100 cm^{-1}) represents the dominating feature; it is likely composed of several overlapping sub-bands. At more positive potentials, an additional sharp band, centered around 2080 cm^{-1} (2070-2085 cm^{-1}), becomes clearly visible. The correlated appearance and strength of the sharp 2080 cm^{-1} band, on the one hand, and the Cu—CO vibrations at 280 and 360 cm^{-1}, on the other hand, are visible in all potential series suggesting that these bands are assignable to the same Cu—CO binding mode. In clear contrast, the broad band of intramolecular C≡O stretch vibrations remains without any obvious counterpart in the region of the Cu—CO vibrations, suggesting assignment to CO adsorption modes that are not associated with detectable Cu—CO vibrations. Largely in line with Ref. 48, where similar experimental findings have been reported, we propose the following explanation: The broad intramolecular CO bands observed at potentials ranging from −0.2 to −0.4 V_{RHE} result from binding of CO to the Cu foam surface involving several binding modes, but without the formation of a specific Cu—CO bond ($^*CO^A$). At even more negative potentials, adsorbed $^*CO$ accumulates at the Cu surface until surface reconstruction allows $^*CO$ to occupy undercoordinated defect sites[48] (giving rise to the sharp 2080 cm^{-1} band), which results in strong electronic backdonation from CO to Cu (appearance of Cu—CO bands, $^*Cu^B$).

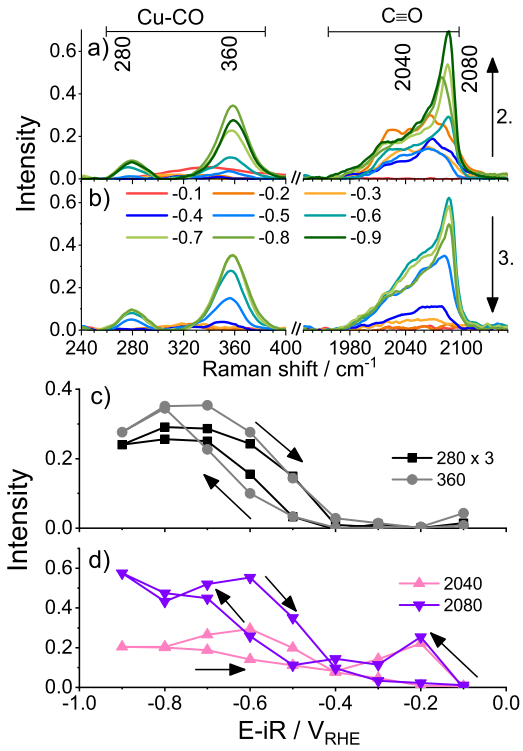

FIG. 6. Potential-dependent intensities of Cu—CO and intramolecular CO bands (in CO_2-saturated 0.1M $KHCO_3$ buffer, pH 6.8). In (a), forward scan from −0.1 to −0.9 V_{RHE} (Series 2 of Fig. 3). In (b), backward scan from −0.8 to −0.1 V_{RHE} (Series 3 of Fig. 3). The arrows indicate the direction of major changes in Raman intensities when decreasing [in (a)] or increasing [in (b)] the electric potential; the legend in panel (b) provides the applied voltages and respective line color. In (c), potential-dependence of the Raman intensity at 280 cm^{-1} and 360 cm^{-1} assignable to Cu—CO bands. In (d), potential-dependence of the Raman intensities at 2040 cm^{-1} and 2080 cm^{-1} assignable to intramolecular CO stretch bands.

Interestingly, $^*CO^A$ is observed already at potentials as high as −0.2 V_{RHE} suggesting CO_2 reduction at surprisingly low overpotentials. However, by gas chromatography (GC) we could detect CO formation only at potentials ≤−0.4 V_{RHE} (Ref. 32 and unpublished results), which renders a correlation of CO formation with $^*Cu^B$ possible. It will be interesting to address in future work the mechanistic role of $^*CO^A$ and $^*CO^B$ in CO_2 reduction.

Based on electrochemical analyses, we recently suggested that a current plateau in cyclic voltammetry (CVs) results from CO_2 reduction and significant $^*CO$ binding to a major fraction of Cu-foam surface sites at potentials more negative than −0.5 V_{RHE}, whereas $^*CO$ desorption requires potentials more positive than −0.4 V_{RHE}.[32] This hypothesis is strongly supported by the herein described hysteresis in the $^*CO$ binding of Fig. 6, in line with results for binding of gaseous CO to copper surfaces.[74]

C. Adsorbed carbonate

In CO_2-saturated $KHCO_3$ with a bulk pH of 6.8, carbonate is mainly present in the form of HCO_3^-; higher pH values shift the equilibrium to CO_3^{2-} [Fig. 7(a), see Fig. S9 for the entire solution spectrum of CO_2-saturated $KHCO_3$ at pH 6.8]. The data of Figs. 7(b)–7(d) imply that bicarbonate on the Cu electrode surface[74] readily undergoes deprotonation;[43] consequently no adsorbed bicarbonate band (C—OH stretching mode at 1015 cm^{-1}) was detected at any electrochemical potentials [Figs. 7(b)–7(d)].

Before and during CO_2RR, we observe carbonate bands at 1070 cm^{-1} (CO_3^{2-} symmetric stretching mode) with a shoulder at 1045 cm^{-1}. The intensity of all the putative carbonate bands shown in Fig. 7 is maximal at the most positive potentials, but their intensities do not change in parallel. Especially in (c), an additional small band at 1130 cm^{-1} is well visible, which exhibits a comparatively weak potential dependence and may be unrelated to adsorbed carbonate species.[75] Interestingly and well visible in (c) and (d), the broad shoulder at 1045 cm^{-1} changes into a distinct band at high potentials. We hypothesize that a second type of carbonate adsorption site is formed during CO_2RR at low potentials that is stably occupied by carbonate only at high potentials.

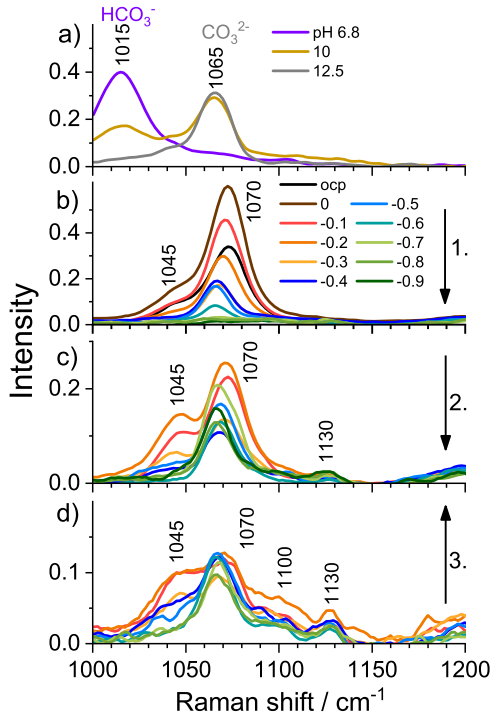

FIG. 7. Carbonate/bicarbonate (CO_3^{2-}/HCO_3^-) Raman bands at 1000-1100 cm^{-1}. (a) Solution spectra of dissolved $KHCO_3$ (0.1M) at pH 6.8 (violet, HCO_3^-), pH 10 (gold), and at pH 12.5 (gray, CO_3^{2-}). [(b)–(d)] *Operando* Raman spectra of the carbonate region at different potentials in 0.1M $KHCO_3$ (pH 6.8) during (b) potential sweep from 0 to −0.9 V_{RHE} (Series 1), (c) second potential sweep from −0.1 to −0.9 V_{RHE} (Series 2), and (d) backward scan from −0.8 to −0.1 V_{RHE} (Series 3). Arrows indicate the scan direction. The legend in (b) provides the applied voltages and the respective line color. All spectra are background subtracted and normalized.

D. C=C and carboxylate vibrations?

The Raman band at 1610 cm^{-1} is present only after Cu oxide reduction (Series 1), before the onset of CO_2RR and at low overpotentials [in Series 2 from −0.3 to −0.7 V_{RHE}, Fig. 3(b)]. Its wavenumber is common for an isolated C=C bond or a C=C bond conjugated with C=O.[71(a)] Previously, this band has been attributed to an ethylene vibration,[46] but the herein observed potential-dependence cannot be reconciled with adsorbed ethylene (Fig. 3). If we do not exchange the electrolyte, accumulation of species produces additional bands in this region at about 1565 and 1677 cm^{-1} (Fig. S10). The vibration at 1610 cm^{-1} could also stem from a carboxylate group ($-CO_2^-$ with strong asymmetric stretch vibration at 1695-1540 cm^{-1} and medium-intensity symmetric stretch vibration at 1440-1335 cm^{-1}).[71(b)]

E. Adsorbed molecules with CH bonds

In the typical $-CH_x$ stretch region, we find Raman bands peaking at 2848, 2874, 2904, 2936, and 2961 cm^{-1} [see Fig. 8(a) for experimental and fitted data at low and higher overpotentials]. During Series 1, if Cu_2O and $Cu-O(H)_{ads}$ are still part of the surface, the $-CH_x$ bands are absent (compare to Fig. 4). They only start to evolve concomitantly to Cu—CO bond formation. During Series 2, the $-CH_x$ bands are observed from −0.2 V_{RHE} on at low intensities, but start to have prominent intensities at <−0.4 V_{RHE}. A band at 2885 cm^{-1} is only distinguishable at <−0.7 V_{RHE}. During Series 3, these species do not desorb completely from the Cu foam surface. If the electrolyte is not exchanged against fresh bicarbonate buffer, the $-CH_x$ species accumulate even more strongly (Fig. S10). We conclude that the adsorption of $-CH_x$ species is not readily reversed at low (non-catalytic) potentials.

For assignment, we compare $-CH_x$ bands during CO_2RR to several reference substances. Distinct assignment of $-CH_x$ species is challenging because of the variety of possible CO_2RR intermediates like *COOH, *CHO, and *COH.[1,76] The mentioned intermediates can arise from several reaction products. The here investigated Cu foams produce formate at high yields at low overpotentials, considerable ethylene at high overpotentials, and small amounts of ethanol, propanol, and ethane (see Ref. 32 for the potential dependent product distribution). Significant methane production on the Cu foams is observed only at very high overpotentials (−1 V_{RHE}), explaining why we detected no methane bands [if present, methane bands are predicted to be at 2917 (strong) and 1534 cm^{-1}].[77]

Reference spectra of possible reaction products are shown in Figs. 8(b)–8(d). We recorded spectra of (i) diluted solutions of methanol, ethanol, formate, formic acid, acetic acid (Fig. S11), and (ii) their possible adsorption onto a Cu foam

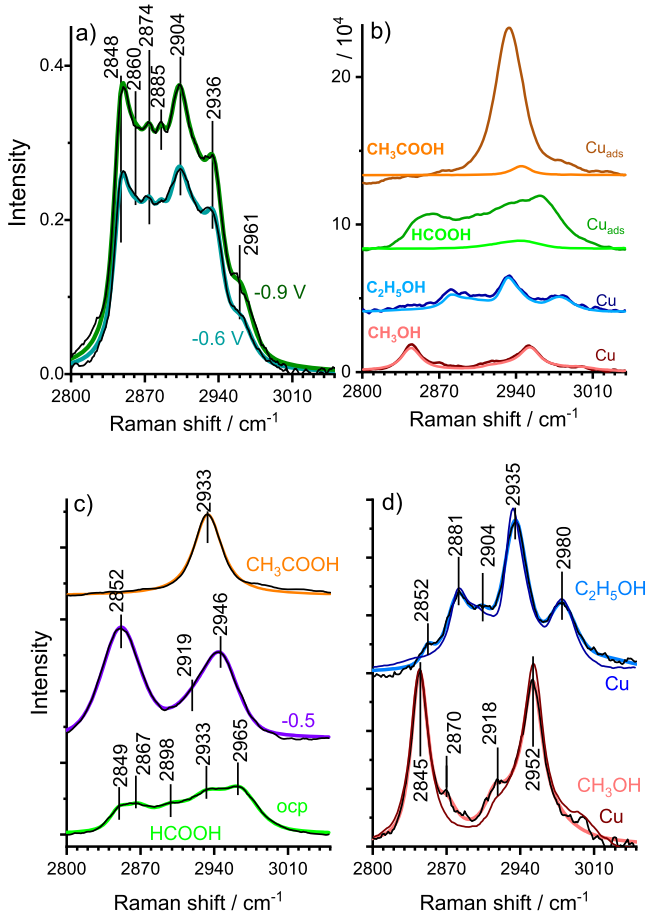

FIG. 8. Raman spectra of the —CH region. (a) Electrochemical CO_2 reduction in CO_2 saturated 0.1M $KHCO_3$ of a Cu foam at −0.6 and −0.9 V_{RHE}. (b) Aqueous solutions (bright lines) of CH_3OH, C_2H_5OH, HCOOH, and CH_3COOH, and a Cu foam surface in 0.1M KH_2PO_4/K_2HPO_4 with reactant at *ocp* (dark lines). [(c) and (d)] Cu foam surface in 0.1M KH_2PO_4/K_2HPO_4 with (c) HCOOH at *ocp* and −0.5 V_{RHE} or CH_3COOH at *ocp*, (d) CH_3OH or C_2H_5OH at *ocp* (thick colored lines) and CH_3OH or C_2H_5OH solutions (thin colored lines). [(a), (c), and (d)] Spectra are background subtracted and normalized (black lines—experimental data and colored lines—fitted data).

surface at an open-circuit potential (*ocp*) in a diluted aqueous phosphate solution containing up to 10% of the respective compound. If we compare the intensities of the diluted solution spectra with the ones at a Cu foam surface at *ocp* [Fig. 8(d)], we observe an intensity-enhancement effect (SERS) for CH_3COOH and HCOOH, indicating adsorption of these species on the Cu surface. Moreover, their Raman spectra change significantly upon adsorption to the Cu surface resulting in several neighboring bands that are not observed in the solution spectra. By contrast, the solution spectra of CH_3OH and C_2H_5OH have similar intensities to the ones of Cu foam at *ocp* suggesting that CH_3OH and C_2H_5OH do not adsorb strongly at the Cu foam surface. In general, the C—H bands of all reference compounds are similar to bands observed for the Cu foam at catalytic potentials (Table S4).

At negative potentials, we see clear indications that formic acid is electrochemically modified. The similarity of the Raman spectra suggests reduction to methanol[78] [Fig. 8(c)]. Acetic acid adsorbs over a wide potential range (with concomitant H_2 evolution[79]) in acetic acid/phosphate solution (Fig. S13 and Table S6). The simulation results providing the peak positions of all investigated species in the typical $—CH_x$ stretching range are summarized in Table S4.

Currently we are not able to assign the $—CH_x$ bands during CO_2RR on a Cu foam to distinct intermediates or products. The comparison of formic acid in solution and its adsorbed counterpart [Fig. 8(b)] illustrates that adsorption can result in different and clearly more complex Raman spectra than observed for the solution species, likely resulting from different adsorption geometries. Similar broad $—CH_x$ modes have been observed before on CuS_x catalysts and have been identified as adsorbed formate.[80] Similarities of the C—H spectra detected for the Cu-foam during and after catalytic CO_2RR operation point toward adsorbed formic acid (or formate) and its reduced form (likely methanol), but we do not observe that the appearance of bands at 1707 cm^{-1} and 892 cm^{-1}, which would be assignable to HCOOH (nor of $HCOO^-$ related O—C—O stretching vibration at 1353 cm^{-1}, Fig. S12), correlate with the magnitude of C—H bands. Thus assignment of CH bands around 2900 cm^{-1} to formic acid (or format) would be in line with the detected Raman spectra only, if the corresponding bands at lower wavenumbers were SERS-silent.

F. Time-dependence of Raman spectra

Time-dependent spectra collected over the course of about 20 min at a constant potential of either −0.5 or −0.7 V_{RHE} exhibit clear differences (Fig. 9). At −0.5 V_{RHE}, we usually do not detect any CO_2RR products via gas chromatography (GC). However, Raman spectroscopy resolves adsorbed surface species, specifically CO and $—CH_x$ species. At −0.5 V_{RHE}, a major fraction of adsorbed species is seen already for data collection starting after 20 s, followed by a slow gradual increase with time.

At −0.7 V_{RHE}, the intensities of the CO and $—CH_x$ bands are constant over the elapsed time, and the small variations reflect the data reproducibility. We thus conclude that at least regarding the CO bands, no accumulation of adsorbed CO (*CO) is detectable. This could be explained by two alternative scenarios:

(i) All accessible CO adsorption sites are occupied within about 20 s so that complete (saturating) *CO coverage is reached.
(ii) The equilibria between catalytic *CO formation, *CO desorption, and CO re-adsorption are reached within about 20 s; these equilibria determine the amount of detectable *CO.

In Ref. 32, we estimated from electrochemical data that a very high, potentially saturating level of *CO is conceivable. Comparison of the *CO peak at 2040/2080 cm^{-1} at −0.5 V_{RHE} and

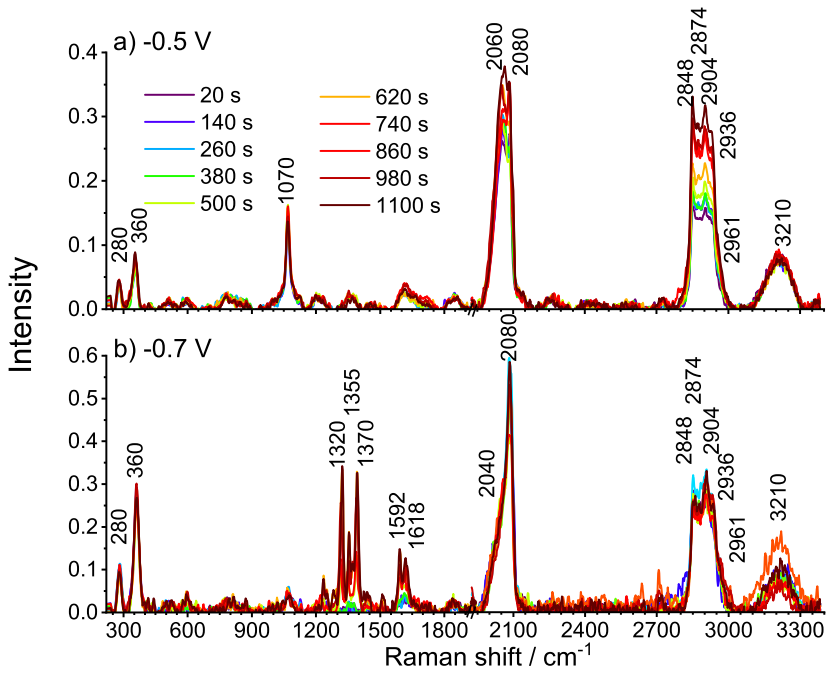

FIG. 9. *Operando* Raman spectra of Cu foam in CO_2-saturated carbonate buffer (0.1M $KHCO_3$ pH 6.8) at (a) −0.5 V_{RHE} and (b) −0.7 V_{RHE} over the course of 20 min. Spectra were collected every 2 min. All spectra are background subtracted and normalized. The noise level increases with an increasing potential due to fierce gas evolution. The time indicated in the legend refers to the starting time of the Raman data collection period.

−0.7 V_{RHE} indeed favors the first scenario of saturated *CO adsorption. If the equilibrium between catalytic *CO formation and net desorption determined the amount of adsorbed CO, then the magnitude (or area) of the *CO peak should be strongly enhanced at −0.7 V_{RHE}, which is not observed. It is a possible consequence of the scenario of saturated *CO coverage that the externally detectable rate of formation of gaseous CO could be limited by the *CO desorption rate. At present, a putative rate limitation caused by saturated *CO adsorption and slow *CO desorption is merely at the level of a working hypothesis. This hypothesis does not yet involve the additional complexity by different *CO adsorption sites (discussed further above) or *CO desorption rates that are potential-dependent or pH-dependent.[74]

A carbonate band at 1070 cm^{-1} is detected at −0.5 V_{RHE} but is almost absent at −0.7 V_{RHE}, which qualitatively is in line with the trend that carbonate bands tend to disappear at more negative potentials. Additional bands at 1320, 1355, and 1370 cm^{-1} are detected for all times ≥500 s at −0.7 V_{RHE}. All bands in between 1310 and 1630 cm^{-1} exhibit the same time dependency. It may be that these bands belonged to a common reaction intermediate with a carboxyl (*COOH) and bidentate COO^- species, similar to suggestions in Ref. 76. A relation of the bands at 1355 cm^{-1} and 1370 cm^{-1} to the carbon dioxide dimer radical described in Ref. 81 is also conceivable, where bands at similar wavenumbers were detected by FTIR spectroscopy (at 1358 and 1368 cm^{-1}, but not at 1320 cm^{-1}). The observed wavenumbers are common for a carboxylate group ($-CO_2^-$ with asymmetric stretch vibration at 1695-1540 cm^{-1} and symmetric stretch vibration at 1440-1335 cm^{-1}),[71(b)] which may stem, e.g., from adsorbed formate or acetate. To explain the slow formation of these bands, we see two alternative options: (i) The formation rate of this product is exceedingly slow so that detectable amounts are accumulated only after about 10 min of CO_2RR or (ii) a slow surface modification is required before a major reaction product is bound in a mode that gives rise to a SERS signal. The former option would be more likely for acetate (essentially no acetate formation detectable[32]), the latter more likely for formate (significant formate formation[32]).

III. CONCLUSIONS

A. Investigating CO_2RR by surface-enhanced Raman spectroscopy (SERS)

1. SERS activity

Cu foams with high electrochemical surface areas (>30 cm^2 per 1 cm^2 of the planar electrode surface) are both interesting catalysts of CO_2RR and excellent SERS-active substrates, bearing the advantage of facile synthesis by a simple electrodeposition protocol. They do not require the employment of any additional surface modification for electrochemical *operando* SERS, thereby ensuring that the SERS-active material is fully identical to the technologically relevant catalyst material.

2. Potential-dependent SERS background signal

A strong background in the Raman spectra complicates the interpretation of specific SERS bands and their intensities seriously. The background intensity depends on the

electric potential as well as the "history" of the surface, e.g., the sequence and duration of the previously applied potential steps. The magnitude of the SERS backgrounds correlates with the strength of the Raman enhancement effect. Therefore, aside from background subtraction also appropriate normalization of the Raman intensities is advisable, which possibly has not been considered in the previous *operando* SERS studies on CO_2RR.

3. Proposed SERS normalization protocol

A simple procedure for the normalization of the SERS spectra is proposed. In the absence of a verified theory on the relation between SERS background and band intensities, we assume proportionality between background and band intensities, which represents a pragmatic, first-order approach. Accordingly, for normalization the SERS spectra are divided by the averaged intensity of the broad featureless SERS background. This approach results in plausible potential dependencies of the Raman band assignable to surface oxides and adsorbed molecular species.

B. Detection of adsorbed molecular species for CO_2-reducing Cu foams

1. Complete reduction of surface oxides

The potential dependence of Raman spectra suggests that surface oxides and hydroxides are present on the as-synthesized Cu foam, but exclusively metallic Cu is present at catalytically relevant potentials. We observe a complete reduction of Cu_2O and possibly mixed oxy-hydroxide phases at about −0.1 V_{RHE}. Three specific vibrational bands, which are likely associated with Cu-bound molecular groups containing carbon and oxygen atoms, are detected only after the reduction of the initial oxide phases and disappear at about −0.4 V_{RHE}.

2. Two distinct CO adsorption modes

There are two basic types of CO adsorption sites. The $^*CO^A$ type is detectable already at surprisingly positive potentials (below −0.1 V_{RHE}) and associated with a broad band of intramolecular CO vibrations (1980-2110 cm^{-1}). Likely, a set of several CO adsorption modes contributes, which are jointly characterized by the absence of any detectable Cu—CO vibrations. The $^*CO^B$ site may be formed by surface reconstruction at potentials below −0.4 V_{RHE}. Its spectroscopic signature comprises one sharp intramolecular CO band (2080 cm^{-1}) as well as two Cu—CO bands (280 cm^{-1} and 360 cm^{-1}).

3. *CO desorption hysteresis and possible relation to the CO formation rate

Clear potential-dependent intensity trends of intramolecular *CO and of Cu—CO bands suggest a hysteresis behavior that supports our previous electrochemical analysis of *CO adsorption/desorption.[32] This hysteresis behavior and indications for saturating *CO coverage of foam surface sites (see Sec. II F) lead to the hypothesis that the *CO desorption characteristics are a co-determinant of the formation rate of externally detectable CO.

4. No HCO_3^- but history-dependent CO_3^{2-} adsorption

There are potential-dependent bands assignable to adsorbed carbonate ions (CO_3^{2-}) at 1070 cm^{-1} with a pronounced shoulder at 1045 cm^{-1} of varying strength. Adsorbed HCO_3^- is not detectable suggesting adsorption-induced deprotonation. When comparing various potential protocols, we do not detect reproducible trends that currently could facilitate data interpretation. Similarly, carboxylate bands potentially assignable to formate or acetate are not consistently detectable for all potential protocols. The occurrence of these bands depends pronouncedly on the history of previous exposures to the electric potential and electrolyte composition. This history-dependence renders conclusions based on a single potential series problematic. Systematic in-depth studies on the conditions for observing carbonate and carboxylate (or carbonyl) bands could be fruitful but are beyond the scope of the present investigation.

5. Variety of species and adsorption modes of CH_x reaction products

Molecular species containing C—H bonds are formed by CO_2 reduction and are clearly detectable as adsorbants on the Cu foam surface as a broad C—H band (2800-3000 cm^{-1}) with minimally six resolvable sub-bands. As opposed to *CO, desorption does not readily occur at non-reducing potentials but requires buffer exchange. Comparison with reference spectra obtained for dissolved molecular species presently do not allow for unambiguous assignment of the adsorbed species, *inter alia* because of pronounced modifications of the Raman spectra upon adsorption to the Cu surface. Adsorbed formate and methanol intermediates may contribute, but also accumulation of potentially interesting reaction intermediates may be visible in the C—H region of the SERS spectrum. Future computational studies could contribute to the identification of the CH_x product species.

6. Complex dependence on catalyst operation history

For all detected CO_2RR products, the Raman bands assignable to adsorbed reaction products depend on the previously applied potential sequences. A fully reversible, hysteresis-free potential dependence is generally not observed. The complex history dependence of the adsorbed reaction products requires more attention. On the one hand, it represents a problematic complication, on the other hand, it provides opportunities. By designing suitable potential protocols, valuable insights into the potential dependent kinetics of product formation, adsorption, and desorption may be obtainable in future investigations.

SUPPLEMENTARY MATERIAL

See supplementary material for details on data collection, data treatment, Cu foam deposition, and additional *operando* Raman data.

ACKNOWLEDGMENTS

We acknowledge financial support from the Bundesministerium für Bildung und Forschung (BMBF, CO2EKAT Project No. 03SF023), the Deutsche Forschungsgemeinschaft (DFG, priority Program No. SPP-1613), and the Chinese Scholarship Council (CSC, Ph.D. fellowship to S.J.). We thank Dr. Luca D'Amario for valuable discussions and help about the data evaluation. We thank Dr. Tintula Kottakkat and Professor Christina Roth (Department of Chemistry, FUB) for joint work on CO_2 reduction by copper foams, and Dr. Stefan Mebs (Department of Physics, FUB) for his support regarding the operation of the Raman spectrometer.

REFERENCES

[1] Z. Wenjun, H. Yi, M. Lianbo, Z. Guoyin, W. Yanrong, X. Xiaolan, C. Renpeng, Y. Songyuan, and J. Zhong, Adv. Sci. **5**, 1700275 (2018).
[2] S. C. Peter, ACS Energy Lett. **3**, 1557–1561 (2018).
[3] J. P. Jones, G. K. S. Prakash, and G. A. Olah, Isr. J. Chem. **54**, 1451–1466 (2014).
[4] M. Gattrell, N. Gupta, and A. Co, J. Electroanal. Chem. **594**, 1–19 (2006).
[5] J. W. Vickers, D. Alfonso, and D. R. Kauffman, Energy Technol. **5**, 775–795 (2017).
[6] J. Schneider, H. Jia, J. T. Muckerman, and E. Fujita, Chem. Soc. Rev. **41**, 2036–2051 (2012).
[7] B. Khezri, A. C. Fisher, and M. Pumera, J. Mater. Chem. A **5**, 8230–8246 (2017).
[8] Q. Lu and F. Jiao, Energy **29**, 439–456 (2016).
[9] F. Li, D. R. MacFarlane, and J. Zhang, Nanoscale **10**, 6235–6260 (2018).
[10] A. H. Shah, Y. Wang, A. R. Woldu, L. Lin, M. Iqbal, D. Cahen, and T. He, J. Phys. Chem. C **122**, 18528–18536 (2018).
[11] H. Mistry, A. S. Varela, S. Kühl, P. Strasser, and B. R. Cuenya, Nat. Rev. Mater. **1**, 16009 (2016).
[12] W. Ju, A. Bagger, G.-P. Hao, A. S. Varela, I. Sinev, V. Bon, B. Roldan Cuenya, S. Kaskel, J. Rossmeisl, and P. Strasser, Nat. Commun. **8**, 944 (2017).
[13] R. Kortlever, J. Shen, K. J. P. Schouten, F. Calle-Vallejo, and M. T. M. Koper, J. Phys. Chem. Lett. **6**, 4073–4082 (2015).
[14] A. J. Gottle and M. T. M. Koper, Chem. Sci. **8**, 458–465 (2017).
[15] F. Calle-Vallejo and M. T. M. Koper, ACS Catal. **7**, 7346–7351 (2017).
[16] R. G. Mariano, K. McKelvey, H. S. White, and M. W. Kanan, Science **358**, 1187 (2017).
[17] A. Verdaguer-Casadevall, C. W. Li, T. P. Johansson, S. B. Scott, J. T. McKeown, M. Kumar, I. E. L. Stephens, M. W. Kanan, and I. Chorkendorff, J. Am. Chem. Soc. **137**, 9808–9811 (2015).
[18] J. T. Feaster, C. Shi, E. R. Cave, T. Hatsukade, D. N. Abram, K. P. Kuhl, C. Hahn, J. K. Nørskov, and T. F. Jaramillo, ACS Catal. **7**, 4822–4827 (2017).
[19] L. Wang, S. A. Nitopi, E. Bertheussen, M. Orazov, C. G. Morales-Guio, X. Liu, D. C. Higgins, K. Chan, J. K. Nørskov, C. Hahn, and T. F. Jaramillo, ACS Catal. **8**, 7445–7454 (2018).
[20] Z. W. Ulissi, M. T. Tang, J. Xiao, X. Liu, D. A. Torelli, M. Karamad, K. Cummins, C. Hahn, N. S. Lewis, T. F. Jaramillo, K. Chan, and J. K. Nørskov, ACS Catal. **7**, 6600–6608 (2017).
[21] K. M. Waldie, F. M. Brunner, and C. P. Kubiak, ACS Sustainable Chem. Eng. **6**, 6841–6848 (2018).
[22] Y. Deng and B. S. Yeo, ACS Catal. **7**, 7873–7889 (2017).
[23] I. E. Wachs and M. Bañares, *Handbook of Advanced Methods and Processes in Oxidation Catalysis* (World Scientific, 2014), pp. 420–446.
[24] Z.-C. Zeng, S. Hu, S.-C. Huang, Y.-J. Zhang, W.-X. Zhao, J.-F. Li, C. Jiang, and B. Ren, Anal. Chem. **88**, 9381–9385 (2016).
[25] Y. Zhang, D. Fu, X. Xu, Y. Sheng, J. Xu, and Y.-f. Han, Curr. Opin. Chem. Eng. **12**, 1–7 (2016).
[26] C. E. Harvey and B. M. Weckhuysen, Catal. Lett. **145**, 40–57 (2015).
[27] X. Li, H.-Y. Wang, H. Yang, W. Cai, S. Liu, and B. Liu, Small Methods **2**, 1700395 (2018).
[28] B. Zhang and J. Zhang, J. Energy Chem. **26**, 1050–1066 (2017).
[29] D. Ren, J. Fong, and B. S. Yeo, Nat. Commun. **9**, 925 (2018).
[30] D. Raciti and C. Wang, ACS Energy Lett. **3**, 1545–1556 (2018).
[31] K. P. Kuhl, E. R. Cave, D. N. Abram, and T. F. Jaramillo, Energy Environ. Sci. **5**, 7050–7059 (2012).
[32] K. Klingan, T. Kottakkat, Z. P. Jovanov, S. Jiang, C. Pasquini, F. Scholten, P. Kubella, A. Bergmann, B. Roldan Cuenya, C. Roth, and H. Dau, ChemSusChem **11**, 3449–3459 (2018).
[33] R. D. Rodriguez, E. Sheremet, M. Nesterov, S. Moras, M. Rahaman, T. Weiss, M. Hietschold, and D. R. T. Zahn, Sens. Actuators, B **262**, 922–927 (2018).
[34] M. Dendisová-Vyškovská, V. Prokopec, M. Člupek, and P. Matějka, J. Raman Spectrosc. **43**, 181–186 (2012).
[35] J. Cejkova, V. Prokopec, S. Brazdova, A. Kokaislova, P. Matejka, and F. Stepanek, Appl. Surf. Sci. **255**, 7864–7870 (2009).
[36] B. Sardari and M. Özcan, Sci. Rep. **7**, 7730 (2017).
[37] M. Moskovits, Rev. Mod. Phys. **57**, 783–826 (1985).
[38] J. T. Hugall, J. J. Baumberg, and S. Mahajan, J. Phys. Chem. C **116**, 6184–6190 (2012).
[39] K. Ikeda, S. Suzuki, and K. Uosaki, J. Am. Chem. Soc. **135**, 17387–17392 (2013).
[40] S. Mahajan, R. M. Cole, J. D. Speed, S. H. Pelfrey, A. E. Russell, P. N. Bartlett, S. M. Barnett, and J. J. Baumberg, J. Phys. Chem. C **114**, 7242–7250 (2010).
[41] K. Q. Lin, J. Yi, J. H. Zhong, S. Hu, B. J. Liu, J. Y. Liu, C. Zong, Z. C. Lei, X. Wang, J. Aizpurura, R. Esteban, and B. Ren, Nat. Commun. **8**, 14891 (2017).
[42] A. Dutta, A. Kuzume, M. Rahaman, S. Vesztergom, and P. Broekmann, ACS Catal. **5**, 7498–7502 (2015).
[43] L. Mandal, K. R. Yang, M. R. Motapothula, D. Ren, P. Lobaccaro, A. Patra, M. Sherburne, V. S. Batista, B. S. Yeo, J. W. Ager, J. Martin, and T. Venkatesan, ACS Appl. Mater. Interfaces, **10**, 8574–8584, (2018).
[44] D. Ren, B. S.-H. Ang, and B. S. Yeo, ACS Catal. **6**, 8239–8247 (2016).
[45] Y. Kwon, Y. Lum, L. Clark Ezra, W. Ager Joel, and T. Bell Alexis, ChemElectroChem **3**, 1012–1019 (2016).
[46] E. A. Batista and M. L. A. Temperini, J. Electroanal. Chem. **629**, 158–163 (2009).
[47] B. D. Smith, D. E. Irish, P. Kedzierzawski, and J. Augustynski, J. Electrochem. Soc. **144**, 4288–4296 (1997).
[48] C. M. Gunathunge, X. Li, J. Li, R. P. Hicks, V. J. Ovalle, and M. M. Waegele, J. Phys. Chem. C **121**, 12337–12344 (2017).
[49] M. B. Ross, C. T. Dinh, Y. Li, D. Kim, P. De Luna, E. H. Sargent, and P. Yang, J. Am. Chem. Soc. **139**, 9359–9363 (2017).
[50] Y. Ichinohe, T. Wadayama, and A. Hatta, J. Raman Spectrosc. **26**, 335–340 (1995).
[51] I. Oda, H. Ogasawara, and M. Ito, Langmuir **12**, 1094–1097 (1996).
[52] A. Ge, P. E. Videla, G. L. Lee, B. Rudshteyn, J. Song, C. P. Kubiak, V. S. Batista, and T. Lian, J. Phys. Chem. C **121**, 18674–18682 (2017).
[53] D. K. Lambert, Electrochim. Acta **41**, 623–630 (1996).
[54] P. Zhang, J. Cai, Y.-X. Chen, Z.-Q. Tang, D. Chen, J. Yang, D.-Y. Wu, B. Ren, and Z.-Q. Tian, J. Phys. Chem. C **114**, 403–411 (2010).
[55] J. Timper, J. Billmann, A. Otto, and I. Pockrand, Surf. Sci. **101**, 348–354 (1980).
[56] D. E. Irish, L. Stolberg, and D. W. Shoesmith, Surf. Sci. **158**, 238–253 (1985).
[57] A. Dutta, M. Rahaman, N. C. Luedi, M. Mohos, and P. Broekmann, ACS Catal. **6**, 3804–3814 (2016).
[58] T. N. Huan, P. Simon, G. Rousse, I. Genois, V. Artero, and M. Fontecave, Chem. Sci. **8**, 742–747 (2017).
[59] S. Sen, D. Liu, and G. T. R. Palmore, ACS Catal. **4**, 3091–3095 (2014).
[60] S. Min, X. Yang, A.-Y. Lu, C.-C. Tseng, M. N. Hedhili, L.-J. Li, and K.-W. Huang, Nano Energy **27**, 121–129 (2016).
[61] S. Anshu, R. P. Mrinal, R. Rekha, T. P. Kodanthakurup, L. Ingo, and K. T. Avesh, Eur. J. Inorg. Chem. **2013**, 2640–2651.
[62] Y. Deng, A. D. Handoko, Y. Du, S. Xi, and B. S. Yeo, ACS Catal. **6**, 2473–2481 (2016).

[63]T. H. Tran and V. T. Nguyen, Mater. Sci. Semicond. Process. **46**, 6–9 (2016).
[64]T. Sander, C. T. Reindl, M. Giar, B. Eifert, M. Heinemann, C. Heiliger, and P. J. Klar, Phys. Rev. B **90**, 045203 (2014).
[65]X. K. Chen, J. C. Irwin, and J. P. Franck, Phys. Rev. B **52**, R13130–R13133 (1995).
[66]H. Hagemann, H. Bill, W. sadowski, E. Walker, and M. François, Solid State Commun. **73**, 447–451 (1990).
[67]A. P. Litvinchuk, A. Möller, L. Debbichi, P. Krüger, M. N. Iliev, and M. M. Gospodinov, J. Phys.: Condens. Matter **25**, 105402 (2013).
[68]U. Collisi and H.-H. Strehblow, J. Electroanal. Chem. Interfacial Electrochem. **284**, 385–401 (1990).
[69]S. González, M. Pérez, M. Barrera, A. R. González Elipe, and R. M. Souto, J. Phys. Chem. B **102**, 5483–5489 (1998).
[70]I. V. Chernyshova, P. Somasundaran, and S. Ponnurangam, Proc. Natl. Acad. Sci. U. S. A. **115**, E9261–E9270 (2018).
[71](a) G. Socrates, *Infrared and Raman Characteristic Group Frequencies*, 3rd ed. (Wiley, 2004), p. 71; (b) p. 128.
[72]W. Akemann and A. Otto, J. Raman Spectrosc. **22**, 797–803 (1991).
[73]W. Akemann and A. Otto, Surf. Sci. **287-288**, 104–109 (1993).
[74]A. Wuttig, C. Liu, Q. Peng, M. Yaguchi, C. H. Hendon, K. Motobayashi, S. Ye, M. Osawa, and Y. Surendranath, ACS Cent. Sci. **2**, 522–528 (2016).
[75]J. D. Frantz, Chem. Geol. **152**, 211–225 (1998).
[76]S. Zhu, B. Jiang, W.-B. Cai, and M. Shao, J. Am. Chem. Soc. **139**, 15664–15667 (2017).
[77]G. Magnotti, U. Kc, P. L. Varghese, and R. S. Barlow, J. Quant. Spectrosc. Radiat. Transfer **163**, 80–101 (2015).
[78]A. Schizodimou, I. Kotoulas, and G. Kyriacou, Electrochim. Acta **210**, 236–239 (2016).
[79]T. Tran, B. Brown, S. Nešić, and B. Tribollet, Corrosion **70**, 223–229 (2014).
[80]Y. Deng, Y. Huang, D. Ren, A. D. Handoko, Z. W. Seh, P. Hirunsit, and B. S. Yeo, ACS Appl. Mater. Interfaces **10**, 28572–28581 (2018).
[81]H. Sheng, M. H. Oh, W. T. Osowiecki, W. Kim, A. P. Alivisatos, and H. Frei, J. Am. Chem. Soc. **140**, 4363–4371 (2018).